

LU TP 10-03
MCnet/10/03
February 15, 2010

Inclusion of Parton Distribution Functions in PYTHIA8

Tomas Kasemets

Master Thesis in Theoretical High Energy Physics
Department of Astronomy and Theoretical Physics, Lund University
Sölvegatan 14A, SE 223 62 Lund, Sweden

Thesis Advisor: Torbjörn Sjöstrand

Abstract

A selection of the latest and most frequently used PDFs is incorporated in PYTHIA8, including the MC-adapted PDFs from the MSTW and CTEQ collaborations. This thesis examines the differences in PDFs as well as the effect they have on results of simulations. The results are also compared to data collected by the CDF experiment.

Contents

1	Introduction	3
2	Quantum Chromo Dynamics	3
2.1	Running Coupling	4
2.2	Cross Section	4
3	Monte Carlo Generators	6
4	Parton Distribution Functions	8
4.1	Monte Carlo-Adapted PDFs	9
5	PDFs in PYTHIA8	9
5.1	MRST/MSTW	11
5.2	CTEQ 6/MC	12
6	Comparison of PDFs	13
7	Minbias Events	14
7.1	Introduction	14
7.2	Multiplicity and Tuning	15
7.3	Results	18
7.3.1	Comparison to CDF Run 2 data	22
8	Inclusive Jet Cross Section	24
8.1	Introduction	24
8.2	Results	26
9	Summary and Conclusions	29
10	Acknowledgments	33

1 Introduction

In order to learn more about the inner essence of nature, particle physicists smash together small particles, such as protons, at large energies, and use huge detectors to detect whatever comes out. The higher the energy, the smaller distances can be examined, which also means that nature at smaller scales can be studied and reveal its secrets. The story is in fact much more complicated.

The protons that clash together are composite particles made up by quarks and gluons that cannot be isolated and studied in their own, but are always confined inside the proton. The collision between two protons is therefore better described as a collision of two approaching bunches of particles, and for the outcome to tell us about nature we need to know what takes part in the collision. Therefore, so called parton distribution functions (PDFs) describe how the momentum of the proton is shared between partons, i.e. quarks and gluons. The PDFs make up one of the ingredients of computer simulations, which combine theories and models in order to predict the outcome, and make it possible to test theory against experiment.

In this thesis we have included the very latest parton distribution functions in the Monte Carlo event generator PYTHIA8 [1]. We compare them and examine how the difference in PDFs affect results of simulations. We also compare the results to real data collected by experiments at Tevatron [2] and examine how the differences change when increasing the energy up to the level of a fully operational LHC (14 TeV) [3].

The structure of the thesis is as follows. In section 2 we introduce some of the concepts of the theory of strong interactions, Quantum Chromo Dynamics (QCD). In section 3 we move on to describe Monte Carlo generators (such as PYTHIA8) and section 4 tells the story of parton distribution functions. Section 5 describes how the PDFs were included in PYTHIA8 and we compare the different PDFs in section 6. Subsequently we study results from simulations of minimum bias events and hard QCD events in section 7 and 8 respectively. Finally we conclude with summary and conclusions in section 9.

2 Quantum Chromo Dynamics

The Standard Model of particle physics is the joint theory of three of the four fundamental forces of nature: electromagnetism, weak and strong force. The part describing the strong interactions, Quantum Chromo Dynamics, is responsible for holding together protons and neutrons in the nucleus as well as quarks inside the nucleons. The strong force is mediated by gluons, which interact with particles that carry color charge, and it grows stronger with distance. Colored particles are therefore confined inside colorless hadrons such as the proton and can never be observed and studied as free particles.

Most calculations in QCD rely on a perturbative expansion in the coupling of the theory. Perturbative QCD uses the Feynman diagrams and rules to calculate matrix

elements and thereby obtain cross sections for different processes. This technique relies on the coupling of the strong force, α_S , to be small enough to make the expansion converge and allow the first terms to be a good approximation. At high energies the strong force is weak, the quarks experience asymptotic freedom and the approximation of truncating the expansion at low orders is good. As one moves down to lower energy, increasingly higher orders would be required, but the perturbation expansion in α_S quickly becomes very complicated and at small enough scales it finally breaks down completely. There are many possible Feynman graphs for each process and all of them will contribute to the cross section. At next-to-leading order the diagrams start to involve loops which introduce integrals over the phase space of the internal lines. These loop integrals diverge, but at each order the real (extra particle in the final state) and virtual (extra particle internal) divergences combine, in a far from trivial way, to cancel out all infinities and leave finite results. This results in very complicated calculations and therefore many processes have only been calculated to leading order. The matrix element calculation gives rise to divergences in two cases, when two partons are collinear and when the energy of a parton is small, soft divergence. How accurate the approximation of the low order expansion is depends on the size of the coupling α_S .

2.1 Running Coupling

The running of the coupling, $\alpha_S = \frac{g^2}{4\pi}$, is necessary in order to absorb infinities in the theory. This is called renormalization and the running is determined by the renormalization group equation [4]

$$\frac{d}{d \log(Q/M)} g = \beta(g), \quad (1)$$

where

$$\beta(g) = -\frac{b_0}{(4\pi)^2} g^3 - \frac{b_1}{(4\pi)^4} g^5 + \dots \quad (2)$$

The two constants depend on the number of flavors, n_f , that have their threshold below the energy scale, $b_0 = 11 - \frac{2}{3}n_f$ and $b_1 = \frac{153-19n_f}{2\pi(33-2n_f)}$. Solving this equation and introducing the mass scale Λ yields

$$\alpha_s(Q^2) = \frac{4\pi}{b_0} \frac{1}{\log(Q^2/\Lambda^2)} - \frac{4\pi b_1}{b_0^3} \frac{\log \log(Q^2/\Lambda^2)}{(\log(Q^2/\Lambda^2))^2} + \dots \quad (3)$$

The first term is the first order expression and the dots are terms that decrease in relative importance for large Q^2 . From this it can be seen that α_S decreases at large Q^2 as $1/\log(Q^2)$ and therefore become very small, but also that the coupling increases towards infinity as Q^2 approaches Λ^2 .

2.2 Cross Section

The cross section describes how likely it is that an interaction will take place. In the regions where the matrix elements can be calculated these give the cross sections for

hard sub-processes, such as $q(p_1)g(p_2) \rightarrow q(p_3)g(p_4)$. To describe the cross section for the sub-process we introduce the Mandelstam variables,

$$\hat{s} = (p_1 + p_2)^2 \quad (4)$$

$$\hat{t} = (p_1 - p_3)^2 \quad (5)$$

$$\hat{u} = (p_2 - p_3)^2, \quad (6)$$

where p_1 - p_4 are the four-momenta of the particles. The differential cross section is given by

$$\frac{E_3 E_4 d^6 \hat{\sigma}}{d^3 p_3 d^3 p_4} = \frac{1}{2\hat{s}} \frac{1}{16\pi} \sum \bar{|\mathcal{M}|^2} \delta^4(p_1 + p_2 - p_3 - p_4), \quad (7)$$

where E_3 and E_4 are energies of the two outgoing partons and the δ -function ensures conservation of energy and momentum. \sum is the sum (average) over initial- (final-) state spins and colors. \mathcal{M} is the matrix element and for the $qg \rightarrow qg$ process, assuming massless partons,

$$\frac{1}{g^4} \sum \bar{|\mathcal{M}|^2} = + \frac{\hat{s}^2 + \hat{u}^2}{\hat{t}^2} - \frac{4}{9} \frac{\hat{s}^2 + \hat{u}^2}{\hat{s}\hat{u}}, \quad (8)$$

to leading order. The sub-process cross section, $\hat{\sigma}(\hat{s}, \hat{t}, \alpha_S(Q^2), \mu^2)$, is a function of the momenta of the partons, the value of the strong coupling at a relevant energy scale Q of the process and the factorization scale μ . μ can be seen as the scale which separates long- and short-distance physics [5], i.e. partons with transverse momentum less than μ are considered as part of the proton and are absorbed into the PDF. The standard choice is to set $\mu = Q$ [4], [6].

Assuming no p_\perp of the interacting partons, the center-of-mass energy squared for the entire collision, s , and for the colliding sub-system, \hat{s} , are related by

$$\hat{s} = (x_1 P_1 + x_2 P_2)^2 \approx x_1 x_2 s. \quad (9)$$

Hence the product $x_1 x_2$ determines the energy fraction available in the sub-process, while the ratio gives the rapidity

$$y = \frac{1}{2} \ln \left(\frac{x_1}{x_2} \right), \quad (10)$$

and thereby determines the direction of motion of the colliding sub-system. In large rapidity events the interacting partons therefore have very different momentum fractions. The average transverse momentum is often good as an energy scale of the process and an upper limit on the transverse energy, p_\perp , is set by the energy available in the subprocess

$$p_\perp^2 \leq \frac{x_1 x_2 s}{4}, \quad (11)$$

with equality only for back to back scattering of two partons perpendicular to the beam axis. In minimum bias events a typical $p_\perp = 2$ GeV, setting a lower limit on the product, $x_1 x_2 \geq \frac{4p_\perp^2}{s} \sim 10^{-7}$ at the LHC, for such an event.

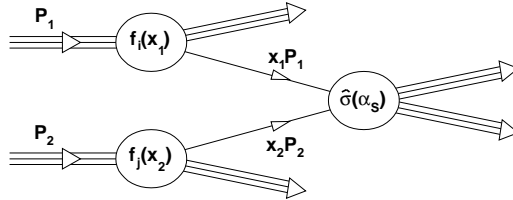


Fig. 1: Two incoming protons with momentum P_1 and P_2 . One parton from each respective proton, with momentum fractions x_1 and x_2 , take part in a hard scattering sub-process producing final-state particles.

The cross section from the matrix element calculations diverge as

$$\frac{d\sigma}{dp_{\perp}^2} \sim \frac{1}{p_{\perp}^4}, \quad (12)$$

when $p_{\perp} \rightarrow 0$. This must be regularized for low transverse momentum which is accomplished by introducing a parameter, $p_{\perp 0}$, (to be discussed more in section 7) such that

$$\frac{d\sigma}{dp_{\perp}^2} \sim \frac{1}{(p_{\perp}^2 + p_{\perp 0}^2)^2}. \quad (13)$$

To obtain the total cross section for the process when two protons collide the probability to find the partons with momentum fraction x inside the proton have to be taken into account, see Fig. 1. The total cross section is then obtained by summing over the different possible partons and integrating over the allowed momentum fractions x ,

$$\sigma(P_1, P_2) = \sum_{ij} \int dx_1 dx_2 f_i(x_1, Q^2) f_j(x_2, Q^2) \hat{\sigma}(x_1 P_1, x_2 P_2, \alpha_S) \quad (14)$$

where P_1 and P_2 are the momenta of the two incoming protons. f_i is the parton distribution function of parton i , which will be described in more detail in section 4.

3 Monte Carlo Generators

Experiments such as proton collisions at high energy are too complicated to make predictions based solely on calculations from first principles of the Standard Model and therefore one has to rely on Monte Carlo generators. The generators start with a central hard collision and then combine matrix elements, parton showers, multiple parton-parton interactions and hadronization models to predict the outcome.[7]

As described in the previous chapter, matrix-element calculations do not describe QCD accurately over the entire phase space. In regions where higher order terms are

necessary to give good approximations the MC generators use the technique of parton showers, which approximates the higher order terms. At each step in the shower the emission probability is calculated and an emission is generated, building up an event with many outgoing partons. This method is a good approximation when the shower can be strongly ordered, i.e. the ordering variable such as virtuality decreases with each emission. That is the case for the largest part of the cross section but not for the hard interactions, where outgoing partons escape at large angles [8]. The parton showers can be subdivided into two types, initial-state radiation (ISR) and final-state radiation (FSR). As the names suggest, ISR describes how the incoming proton branches into many quarks and gluons before the collision while FSR takes the products of the collision and describes how they branch into more particles. FSR is evolved in strictly ordered virtuality where at each step the virtuality is smaller than in the previous. ISR is more complicated. It is ordered in increasing virtuality but since the simulation starts with the hard interaction the ISR has to be evolved backwards [9]. This backward evolution of ISR is one of the most challenging parts of a generator [10].

The showers and matrix elements are good approximations in two entirely different regions. Matrix elements are good for hard collisions, producing particles at large transverse momentum while parton showers are good at low energies and for collinear partons. In order to make use of their respective advantages they need to be matched at some energy scale to cover the entire phase space and in a way that assures there is no double counting [11], [8].

PYTHIA8 uses showers ordered in p_{\perp} which has an advantage over mass ordered showers (which were used in the previous version PYTHIA6.4 [12]) because it automatically takes care of some effects due to coherence between emissions. These, however, are not the only possible choices and for example HERWIG [13], the other large general Monte Carlo generator, uses energy weighted angular ordering. This has advantages related to coherence effects but can not be used over the full phase space and hence leaves some regions to be filled in by high order matrix elements [10].

After the FSR the hadronization starts, and the partons produced in the previous stages split up and combine into colorless hadrons than can survive and possibly reach a detector. It is also at this level that experiments collect their data. The hadronization has not yet been possible to determine from the theory and therefore models are required. PYTHIA8 uses the Lund string model [14] where partons tie color connections to each other which break by forming quark–antiquark pairs, while HERWIG uses cluster fragmentation [15].

There is no reason why, in a proton collision, there should only be one parton from each proton that interacts, and in fact it is not even the case most of the time. Therefore the so called multiple interaction framework simulates the additional interactions. As the collision energy increases, partons at smaller x become involved and more particles can be produced in the ISR. Multiple interactions are therefore increasing and the models for multiparticle interactions are put to the test as the energy at LHC rises.

PDFs are used in Monte Carlo generators at several stages. First in calculating the cross section for the hard collision to take place, which we have seen in eqn. 14. Secondly, ISR use the PDFs since it is the partons inside the proton that will shower, so the PDFs are needed to describe what we have to start with and is used in the backwards evolution of the ISR. Finally, PDFs also enter through cross section calculations in the multiple interactions framework.

4 Parton Distribution Functions

The static properties of the proton are dominated by the valence quarks, i.e. two up quarks and one down quark. The dynamic picture of the proton is less simple. Quarks interact by exchanging gluons, which can split up into quark–antiquark pairs and send out additional gluons. The proton thus consists of three valence quarks, gluons and sea quarks which all go under the common name of partons. Parton distribution functions (PDFs) describe how the momentum of the proton is distributed among partons and at leading order they can be interpreted as the probability to find a parton inside the proton with a certain momentum fraction. At higher order this simple picture fails since, for example, the NLO PDFs can be negative.

There are six quarks with antiquarks and adding the gluon, the proton has, potentially, 13 PDFs. However, the heavy top quark/antiquark is not included taking the number down to eleven. When a gluon splits it is always into a quark–antiquark pair, and hence the distributions of quarks and antiquarks should be the same (once the valence quarks are excluded). Therefore strange, charm and bottom quarks used to be considered to have exactly the same distribution as their respective antiquark, setting the total number of distributions to 8. However this is not necessarily true and this symmetry can be broken, which is also the case (at least) for the strange quark/antiquark. The proton can be seen as accompanied by a kaon cloud, since the proton can split into a $\Lambda(uds)$ and a $K^+(u\bar{s})$, where the s quark sits in the first and the \bar{s} in the second. There is no reason to believe that the s quark in the Λ should have the same momentum as the \bar{s} in the K^+ [16]. Therefore some of the newer PDFs have a small difference between the two distributions.

The PDFs obey a number of relations such as the the momentum sum rule

$$\int_0^1 dx \sum_i x f_i(x) = 1, \quad (15)$$

where the sum is over all partons in the PDF, which states that the total momentum of all the partons must equal the momentum of the proton.

The PDFs are functions of the fraction of the proton's momentum x carried by the parton and of Q^2 , which can be interpreted as a measure of resolving power. Once the parton distributions are known for one specific Q^2 , they can be evolved to higher Q^2 by use of the DGLAP equation [17]

$$\frac{\partial f_i(x, Q^2)}{\partial Q^2} = \frac{\alpha_s}{2\pi} \sum_j \int_x^1 \frac{dy}{y} f_j(y, Q^2) P_{j \rightarrow i} \left(\frac{x}{y} \right), \quad (16)$$

where f_q is the parton distribution function for parton q and $P\left(\frac{x}{y}\right)$ is the splitting function.

The outcome of experiments depend on how the momentum is distributed but there is no way to directly calculate what the distribution should be. Therefore several groups work on parameterizing and fitting PDFs to available data [18]-[21]. The large x behavior of the PDFs are constrained by fixed target experiments. At smaller x the constraints come from deep inelastic scattering (DIS) at electron-proton colliders such as HERA. The DIS data have high statistics and therefore dominate the PDF fits. This gives good knowledge of the quark distributions but the gluon distribution is harder to obtain, since gluons do not directly interact with electrons. In hadron colliders the picture is much more messy, since there is now two composite particles and the gluon distribution is therefore the least constrained part of the PDFs. For more details on the data sets of PDF fits see [22] and [18].

4.1 Monte Carlo-Adapted PDFs

There are PDFs of several different orders, LO, NLO and some NNLO. The general-purpose generators are all leading order and therefore one would like to combine them with leading-order PDFs. However, we know for example that higher orders generally give positive contributions to cross sections and in recent years some modified LO PDFs have been released, specifically tailored for leading-order Monte Carlo generators. These try to simulate some of the effects of NLO calculations by compensating for known shortcomings of the leading-order. Among other things these PDFs allow for a non-conservation of momentum by relaxing the momentum sum rule, i.e. the partons inside the proton are allowed to have a total momentum larger than the momentum of the proton. This permits the PDFs to grow large in some regions without decreasing in others and thereby simulate the effects of some of the next-to-leading-order corrections, in particular allowing a large value of the gluon distribution at small x without compromising the quark distributions at large x . The MC-adapted PDFs released so far are LO* and LO** [23] from the MRST group and MC1, MC2 and MCS [25] from the CTEQ group. All of them except MCS have relaxed the momentum sum rule. MC1 use a leading-order running of α_S while LO*, LO** and MC2 use next to leading-order running. LO** also has a change in argument, to p_{\perp}^2 rather than Q^2 , for α_S for high- x evolution. MCS has more freedom in the parameterization and allows for change with scale, to simulate NLO cross section calculations (a feature we do not make use of in PYTHIA8). MC1/2/S are all fitted to a combination of real data and NLO pseudo data in an attempt to obtain the ideal PDF for leading-order MC generators.

5 PDFs in PYTHIA8

PYTHIA8 [1] has so far been distributed with the option to choose between two PDFs, GRV94L [26] and CTEQ5L [27], which are both fairly old. Many new and improved

Previous	New	
	MRST/MSTW	CTEQ
GRV94L	MRST LO*	CTEQ6L
CTEQ5L	MRST LO**	CTEQ6L1
	MSTW LO	CTEQ66
	MSTW NLO	CT09MC1
		CT09MC2
		CT09MCS

Tab. 1: PDFs that are now included in PYTHIA8. We included all but two, which were already available in PYTHIA8.

PDFs have been released and made available to PYTHIA8 simulations only through LHAPDF [28]. The LHAPDF package has grown quite large and in that process also a bit slow, also the code is written in Fortran while the community is changing to C++. It is desirable to include some PDFs directly into PYTHIA8 because it can speed up simulations, make PYTHIA8 more complete and make it easier to switch between different frequently used PDFs. Furthermore some of the latest PDFs have not yet been included in LHAPDF. Therefore we incorporate ten new PDFs from the MRST [23]-[24], MSTW 2008 [18], CTEQ6 [19] and CTEQ MC [25] distributions into PYTHIA8. Two of them are NLO which are not intended for MC use, but included for comparison. The main danger with them is for low- p_{\perp} processes. Inclusion of the PDFs was done in cooperation with the MSTW and CTEQ collaborations, [33]-[35], and the PDFs are listed in Tab. 1.

Including additional PDFs proved to be less straightforward than might first be expected. A major reason for this is the need to, in MC simulations, go outside the range of the PDF grids. Specifically we need to go down to smaller x and Q^2 values than many of the distributions. At LHC energies, x values as low as 10^{-8} are desirable, while some of the PDFs only range down to 10^{-6} , and multiple interactions take place at low Q^2 . MSTW provides routines not only for interpolation but also for extrapolation outside this grid while the CTEQ collaboration has recommended a freeze of the PDFs at the value just inside the grid. The range of the grids for the different PDFs are shown in Tab. 2.

The code supplied by the authors had to be modified to fit natively into PYTHIA8 and we also did extensive tests. When possible the tests included comparisons to the corresponding PDFs in the LHAPDF package. We then found that the PYTHIA8 included PDFs run about a factor two faster than they do going the way via the LHAPDF package.

The s and \bar{s} distributions were set equal in previous versions of PYTHIA8 and since that was not the case in some of the new PDFs, P PYTHIA8 was modified to support such a difference. The different PDFs have different values of α_S and also use different orders of the running, as listed in Tab. 2. The PYTHIA8 default is to use first order running for all α_S but this can be changed in the settings and we

PDF	x range	Q^2 range [GeV ²]	α_S	$\alpha_S(M_Z)$
GRV94L	$10^{-5} - 1$	$0.40 - 10^6$	LO	0.128
CTEQ5L	$10^{-6} - 1$	$1.00 - 10^8$	LO	0.127
MRST LO*	$10^{-6} - 1$	$1.00 - 10^9$	NLO	0.12032
MRST LO**	$10^{-6} - 1$	$1.00 - 10^9$	NLO	0.11517
MSTW LO	$10^{-6} - 1$	$1.00 - 10^9$	LO	0.13939
MSTW NLO	$10^{-6} - 1$	$1.00 - 10^9$	NLO	0.12018
CTEQ6L	$10^{-6} - 1$	$1.69 - 10^8$	NLO	0.1180
CTEQ6L1	$10^{-6} - 1$	$1.69 - 10^8$	LO	0.1298
CTEQ66 (NLO)	$10^{-8} - 1$	$1.69 - 10^{10}$	NLO	0.1180
CT09MC1	$10^{-8} - 1$	$1.69 - 10^{10}$	LO	0.1300
CT09MC2	$10^{-8} - 1$	$1.69 - 10^{10}$	NLO	0.1180
CT09MCS	$10^{-8} - 1$	$1.69 - 10^{10}$	NLO	0.1180

Tab. 2: The x and Q^2 ranges of the grids for the different parton distribution functions, as well as the order of the running of α_S and the value at M_Z .

examine the effects that such a change can have.

5.1 MRST/MSTW

The PDFs supplied to us from MSTW have in some respects been improved compared to the versions available in LHAPDF. Our implementation for the MRST LO* and LO** PDFs make use of the new MSTW grid (64×48) ranging down to $x = 10^{-6}$ while the LHAPDF versions use the original grid with fewer (49×37) grid points and shorter x range (10^{-5}). The values of α_S are a bit different in the new grid files of LO* and LO** than in the corresponding LHAPDF grid files. LHAPDF versions use Λ_{QCD} for four active flavors which introduce possible round off errors while stepping into the five flavor region of $\alpha_S(M_Z)$ and the change to Λ_{QCD} for five active flavors yields a slightly different value for $\alpha_S(M_Z)$. Also worth noticing is that LO* and LO** both use the unorthodox value of the Z boson mass, $M_Z = 91.71$ GeV, unlike the MSTW 2008 distribution which uses $M_Z = 91.19$ GeV [28]. For MSTW 2008 LO the LHAPDF interpolation gave negative values between the last two grid points (as previously discovered by the HERWIG group) in x , i.e. $0.975 \leq x \leq 1$ and we therefore changed to a linear interpolation between the two points. However, the problem at large x values is not limited to the very last interval on the grid but extends over more x values and over a wide range of Q^2 . Both LO* and LO** give negative values of the gluon distribution in several intervals where $x > 0.85$, as shown in Fig. 2. The corresponding LHAPDF PDFs, which use the older grid with fewer grid points also have this problem but not in the same intervals. In simulations with PYTHIA8 any negative PDF value will automatically be put to zero and therefore the negative values of the gluon distribution (where it is very small) do not affect the results of simulations. LHAPDF also gives negative values for the up quark, which is worse since the up quark dominates for these x values. This indicates that

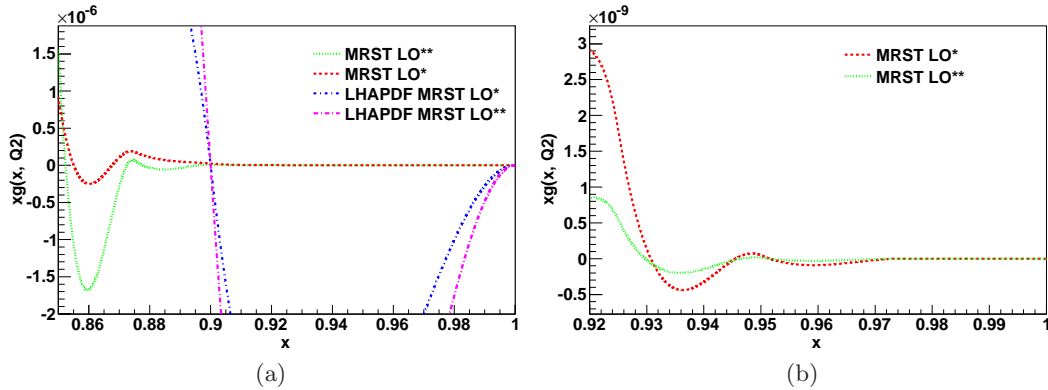


Fig. 2: Negative gluon distributions for large x values.

improvements of the numerical stability are needed in the large x region. We also found a large difference between the two distributions for LO* and LO**, where the old distributions gave much steeper PDFs at small x and at $x = 10^{-8}$ the differences reached a factor of two.

The MSTW NLO distribution gave very large negative values for the anomalous dimension $\frac{d \log(xf)}{d \log(Q^2)}$ at small Q^2 and x -values around 10^{-5} , which resulted in a huge \bar{s} -distribution when extrapolated to low Q^2 . This could also be a problem for the gluon which could get large negative anomalous dimensions in the x region where the distribution is negative. To avoid this the anomalous dimension is manually forced to be larger than -2.5 . Although this does fix this issue at hand, it is also an example of the dangers of using NLO PDFs in LO MC simulations, and an indication that one has to be very careful with such use.

5.2 CTEQ 6/MC

The CTEQ distributions work well inside the grid but outside or near the edges some problems occurred. The $tv = \log(\log(Q))$ values in the grid file were discovered to not exactly correspond to the Q values and hence, some points that were inside the Q grid would end up outside the tv grid. This caused some large issues, for example the b distribution, after being zero below the threshold, suddenly became huge at Q^2 values just inside the grid. Therefore we choose to read in only the Q grid points and then calculate tv .

There can be differences between the CTEQ6 PDFs in PYTHIA8 and the corresponding ones in LHAPDF outside the grid. This is because LHAPDF provides the option to use extrapolation routines where PYTHIA8, by recommendation from the CTEQ authors, freezes the values. The CTEQ MC distributions are not included in the current LHAPDF package, which is therefore, to the best of our knowledge currently available for simulations only in PYTHIA8. To freeze the PDFs can be dangerous both at small x and small Q^2 . The region below Q_{min} is populated by

PDF	Total Momentum Fraction
CTEQ5L	1.00
MRST LO*	1.12
MRST LO**	1.14
MSTW LO	1.00
MSTW NLO	1.00
CTEQ6L	1.00
CTEQ6L1	1.00
CTEQ66	1.00
CT09MC1	1.10
CT09MC2	1.15
CT09MCS	1.00

Tab. 3: The total fraction of the protons momentum held by all the partons for the different PDFs evaluated at $Q^2 = 10^3$.

multiple interactions so simulations are affected by the behavior of the PDFs in this region and some of the PDFs do not range down to small enough x if LHC reaches its full energy. There should be no problems above Q_{max} which is already large enough and in a region where the PDF evolution is slow.

6 Comparison of PDFs

The gluon distribution is dominating in the region of small x while the valence quarks, and then especially the up quarks, dominate for large x . We therefore choose to focus mainly on these two distributions since they will affect the results the most.

The PDFs are different from one another in several aspects and Tab. 3 show that four of them do not obey the momentum sum rule. MC2 carries the largest momentum fraction of 1.15 closely followed by LO** which has the special behavior where the fraction changes with Q^2 as shown in Fig 3a. Although CTEQ5L also changes, see Fig 3b, this is unintentional, because of technical reasons, and the scale of the changes is too small to give any noticeable effects.

Minimum bias events are sensitive to low Q and a Q^2 around 4 GeV^2 is a typical scale for such simulations. Looking at the gluon and up distributions at $Q^2 = 4 \text{ GeV}^2$ in Fig. 4 we see that the up distributions are all similar, with slight differences for the two NLO PDFs and CT09 MC1 and MC2. For the gluon distribution we see large differences at small x values. MSTW LO has a much steeper rise and gets much larger than the others. All the MRST/MSTW distributions give larger values at small x than the CTEQ ones. The MC-adapted PDFs follow each other within both distributions, except for MCS which is more similar to CTEQ6L and CTEQ6L1. The two NLO PDFs stand apart from the rest and MSTW NLO is negative in a large region. One can also see that CTEQ5L, CTEQ6L and CTEQ6L1 all freeze at $x = 10^{-6}$.

Fig. 5 shows the distributions at larger $Q^2 = 10^3$ and here the up distributions

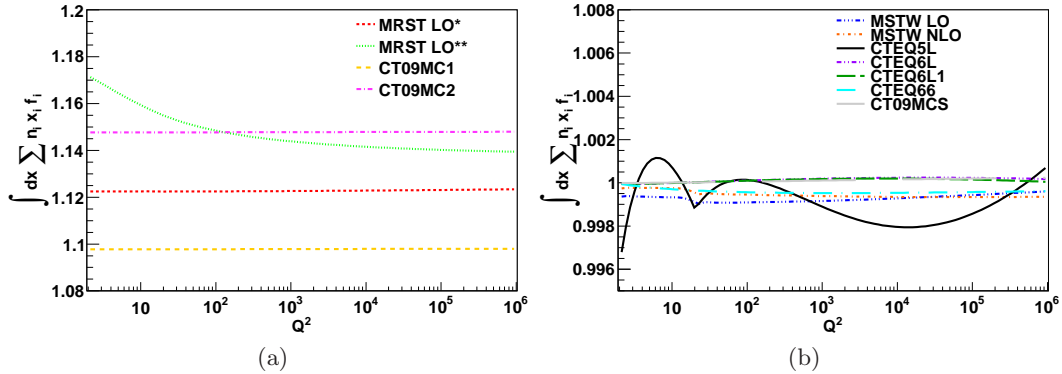


Fig. 3: The momentum fraction held by the partons in different PDFs. To the left are the four PDFs which break the momentum sum rule.

show the same pattern. This is also the case for the gluon distributions. However, the differences between the PDFs are now smaller, and especially the difference between the two groups is no longer as prominent. We can also see in Fig. 5d that all three MC-adapted PDFs from CTEQ are similar at this Q^2 . Taking a look at the \bar{s} in Fig. 6 at an intermediate $Q^2 = 50 \text{ GeV}^2$ we see a similar pattern as we saw for the gluons.

In general the MSTW LO blows up at small x values and is much larger than all the others in this region. The MC-adapted PDFs show strong similarities, especially within their respective collaboration, while MCS stands out by sometimes resembling the ordinary LO PDFs. The similarity between the two NLO PDFs is also clear and CTEQ66 looks similar to MSTW NLO for large Q^2 but does not go negative at $Q^2 = 4 \text{ GeV}^2$. Comparing the two groups the CTEQ distributions have smaller distributions at small x both for the PDFs that freeze, and also for the ones with grid ranging down to 10^{-8} .

7 Minbias Events

7.1 Introduction

In experimental physics minimum bias events are what would be seen in a totally inclusive trigger where everything except elastic and (most) diffractive events is accepted. In PYTHIA8, minbias events are equivalent to inelastic nondiffractive events. They are managed by the multiple interactions machinery and is affected by the PDFs through cross section calculations.

Minbias events tend to have low average transverse energy, low particle multiplicity and consist largely of soft inelastic interactions which are interesting both in their own right and because they constitute background when studying hard inter-

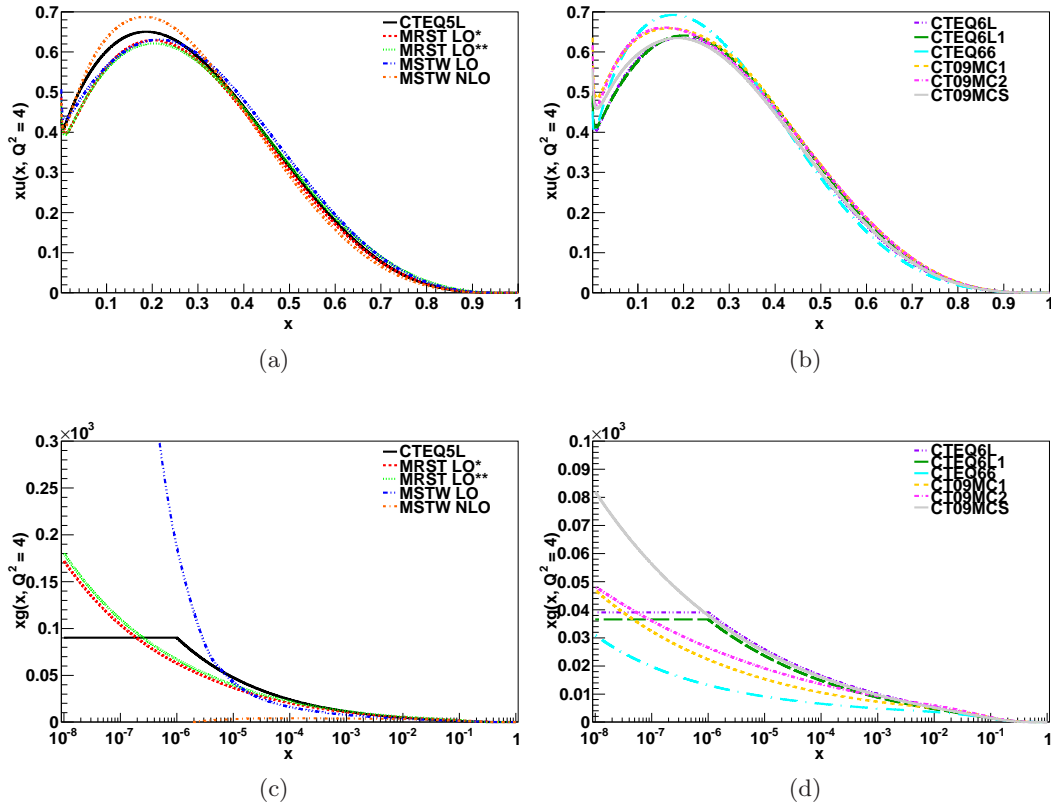


Fig. 4: Up quark (a, b) and gluon (c, d) distributions at $Q^2 = 4 \text{ GeV}^2$. Note difference in horizontal and vertical scales.

actions. Because of the low p_\perp the interacting partons only need a small portion of the momenta of the incoming hadrons, and hence minbias events probe parton distributions in the small x region dominated by the gluon distribution.

We examine the rapidity, multiplicity and p_\perp distributions from simulations with different PDFs, both at Tevatron and LHC energies. With the aid of Rivet [29] we also compare p_\perp and $\sum E_\perp$ particle spectra as well as average p_\perp evolution with multiplicity to real data taken by the CDF experiment at Tevatron Run 2 [30].

7.2 Multiplicity and Tuning

The larger momentum carried by the partons in LO*, LO**, MC1 and MC2 yield a larger activity and hence a larger multiplicity than with the ordinary leading-order PDFs. Furthermore the NLO PDFs give less activity, so before comparing the simulations we first tune PYTHIA8 so that all PDFs have the same average charge particle multiplicity as CTEQ5L. We choose CTEQ5L as reference because it is the default PDF in PYTHIA8 and is most commonly used in PYTHIA8 simulations. We

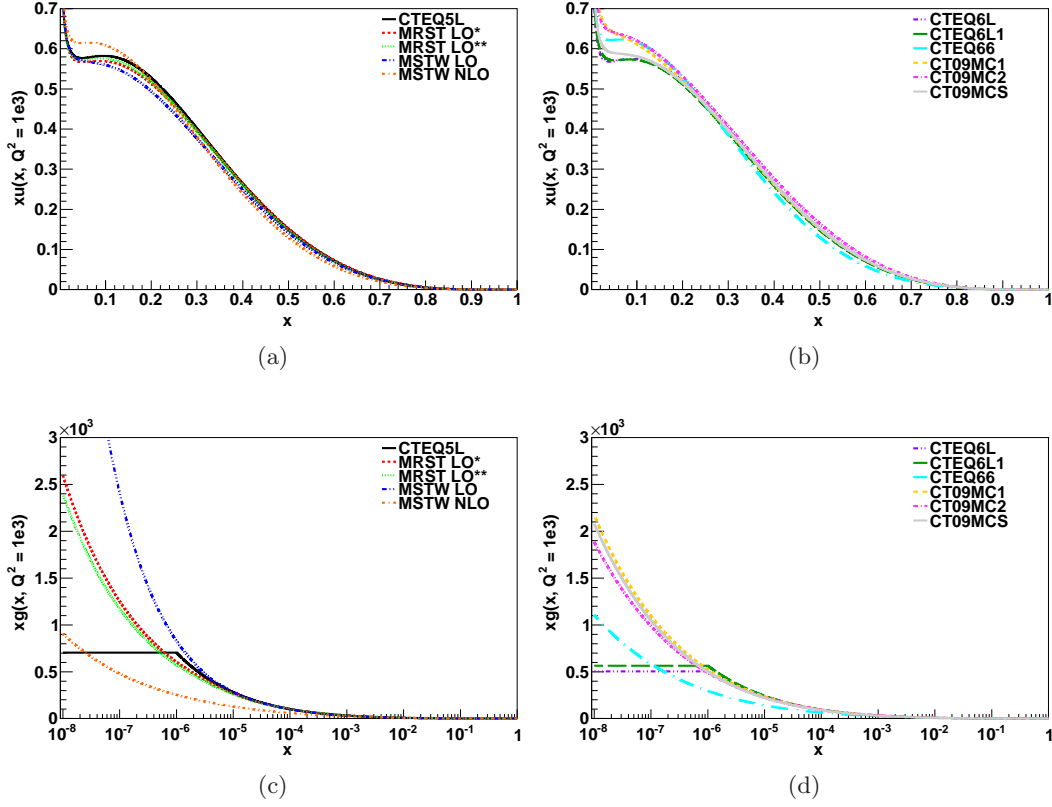


Fig. 5: Up quark (a, b) and gluon (c, d) distributions at $Q^2 = 10^3 \text{ GeV}^2$. Note difference in horizontal and vertical scales.

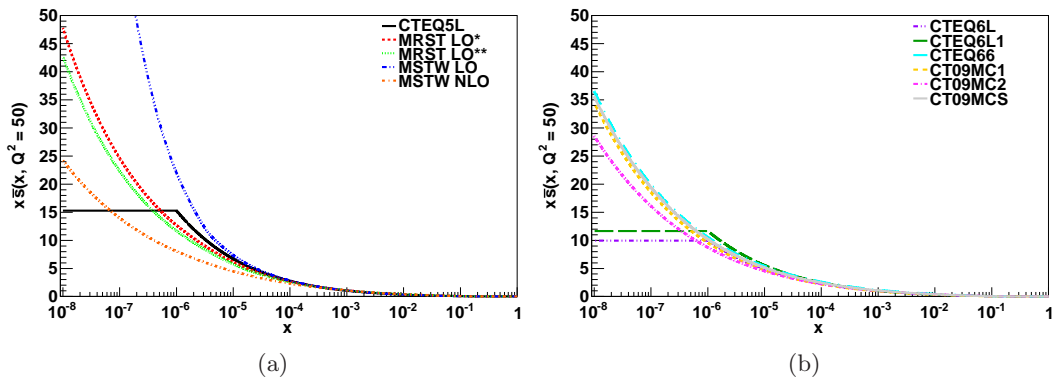


Fig. 6: \bar{s} distributions at $Q^2 = 50 \text{ GeV}^2$.

PDF	Charged Particle Multiplicity	$p_{\perp 0}^{\text{Ref}}$
CTEQ5L	54.48	2.25
MRST LO*	59.74	2.50
MRST LO**	63.52	2.63
MSTW LO	49.10	2.06
MSTW NLO	48.02	1.56
CTEQ6L	54.92	2.25
CTEQ6L1	51.71	2.13
CTEQ66	42.85	1.75
CT09MC1	53.92	2.25
CT09MC2	60.37	2.50
CT09MCS	54.87	2.25

Tab. 4: Average charged particle multiplicity for the different PDFs with the default value of $p_{\perp 0}^{\text{Ref}} = 2.25$ and also the $p_{\perp 0}^{\text{Ref}}$ required to tune the charge multiplicity equal to the value for CTEQ5L.

are not making a complete tune and only intend to get a first impression of relative differences, under comparable conditions. The tuning is accomplished by tweaking the $p_{\perp 0}^{\text{Ref}}$ parameter in PYTHIA8

$$p_{\perp 0} = p_{\perp 0}^{\text{Ref}} \left(\frac{E_{\text{CM}}}{E_{\text{CM}}^{\text{Ref}}} \right)^p \quad (17)$$

where $E_{\text{CM}}^{\text{Ref}} = 1800$ GeV and $p = 0.24$. $p_{\perp 0}$ is used for the regularization of the divergence of the QCD cross section as $p_{\perp} \rightarrow 0$, eqn. 13, and a smaller $p_{\perp 0}$ cause the regularization to kick in at a lower p_{\perp} increasing the charged particle multiplicity, n_{ch} . The simulations were done with 100 000 events and $p_{\perp 0}^{\text{Ref}}$ tuned until the relative difference $\left(\frac{\langle n_{PDF} \rangle - \langle n_{5L} \rangle}{\langle n_{PDF} \rangle + \langle n_{5L} \rangle} \right)$ was less than 1%. The tuning was done for the α_S value and leading-order running which is default in PYTHIA8, as well as with α_S determined individually by the PDFs. Results are shown in Tab. 4 and 5 respectively. With the PYTHIA8 default α_S the largest multiplicity is obtained with LO**, followed by MC2 and LO* which also are the PDFs with most momentum, but 6L manages to squeeze in before MC1 follows. This changes for the α_S determined by the PDFs since MC1 and LO experience a large increase in multiplicity.

For MSTW NLO the integrated interaction cross section is smaller than the nondiffractive inelastic one and therefore PYTHIA8 automatically lowers p_{T0} . This occurs for both NLO PDFs when we use the α_S specific to the individual PDFs and, although this does not cause any trouble, it is a reminder of the danger of using next-to-leading-order PDFs together with leading order MC generators.

PDF	Charged Particle Multiplicity	$p_{\perp 0}^{\text{Ref}}$
CTEQ5L	54.48	2.25
MRST LO*	57.43	2.38
MRST LO**	56.03	2.31
MSTW LO	60.58	2.50
MSTW NLO	46.17	1.31
CTEQ6L	51.11	2.13
CTEQ6L1	54.18	2.25
CTEQ66	43.89	1.63
CT09MC1	62.35	2.50
CT09MC2	55.78	2.31
CT09MCS	50.83	2.13

Tab. 5: Average charged particle multiplicity for the different PDFs with the default value of $p_{\perp 0}^{\text{Ref}} = 2.25$ and also the $p_{\perp 0}^{\text{Ref}}$ required to tune the charge multiplicity equal to the value for CTEQ5L. With α_S value and running set individually.

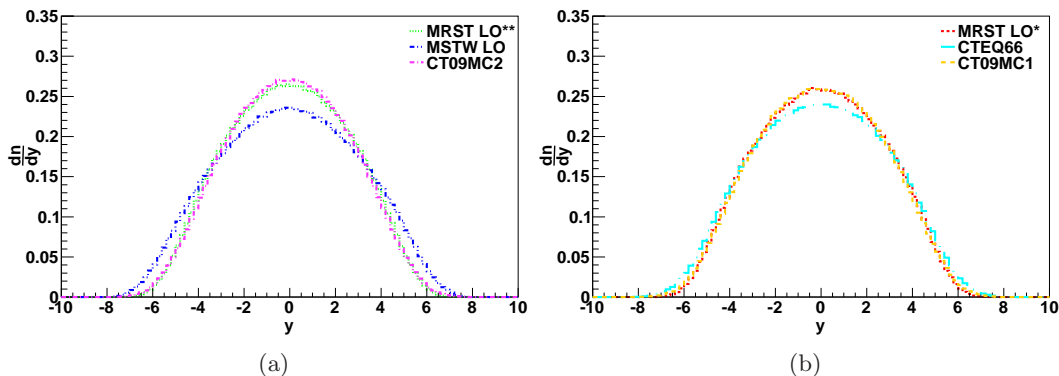


Fig. 7: Rapidity distributions of the partons created in the $2 \rightarrow 2$ sub-process.

7.3 Results

In this section all simulations are done at the CM-energy of 1960 GeV, if not explicitly stated otherwise. So as not to cram the pictures, not all sets are shown all the time. We have tried to choose a selection of PDFs to show in each plot what represents both the extremes and the middle way. The rapidity distributions of the outgoing particles at the parton level when only the $2 \rightarrow 2$ sub-process is considered are presented in Fig. 7. MSTW LO has a broader distribution than the rest of the PDFs with more particles at larger rapidities as an effect of the large gluon distribution at the small x . We can also see that LO** closely resembles MC2, as does LO* and MC1 while the two NLO distributions are lower in the central rapidity region. The remaining leading-order distributions all show similarities to the MC-adapted ones.

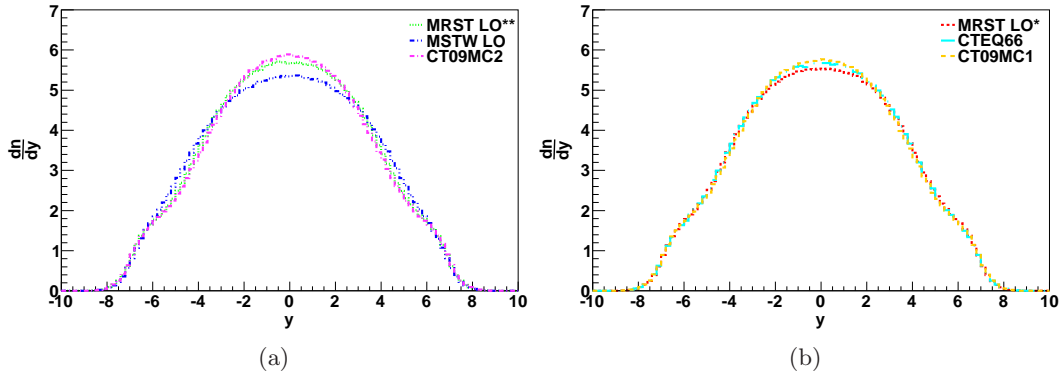


Fig. 8: Rapidity distributions of charged particles after hadronization at minbias simulations with $s = 1960 \text{ GeV}^2$.

Turning on the rest of the PYTHIA8 machinery and looking at the distribution of charged particles after hadronization, shown in Fig. 8, the distribution changes its shape. There are now more particles at larger rapidities as a result of fragmenting color field strings stretched out to the beam remnants and most of the differences between the PDFs get blurred. Some differences still remain and MSTW LO is still smaller for central rapidities, and as a remnant of the wider distribution lack the inward dents that all other PDFs have at rapidities around ± 5 . The peaks of LO** and MC2 are a bit sharper than for LO* and MC1 but the trace of the lower value of the CTEQ66 at central rapidity is gone.

Minimum bias events are dominated by $gg \rightarrow gg$ interactions but if we go back to the partons in Fig. 7 and select only the outgoing quarks, i.e. mainly from $qg \rightarrow qg$, large underlying differences are revealed, see Fig. 9. The CT09 and CTEQ66 distributions show smooth shapes leading up to a peak at zero rapidity, while LO*/** have a very flat distribution at central rapidities. The outlier is once again the MSTW LO distribution which shows peaks at large rapidities. This is once again caused by the large gluon distribution at small x and we believe a reason, that it is so much more prominent for the quarks, is that MSTW LO has a relatively small gluon distribution at large x which in asymmetric qg interactions somewhat compensates, while the up-quark distribution is similar to the other PDFs. The normal LO distributions from CTEQ show similar distributions as the MC-adapted ones from MSTW. Actually CTEQ5L show similar peaks as MSTW LO, and looking at the gluon distribution at low energies we can see that before it freezes as $x = 10^{-6}$ it is larger than in all other PDFs. There is also a clear difference in the amount of quarks produced where CTEQ66 has a much larger amount and thereby produces much more quark initiated jets than the rest of the PDFs.

The multiplicity distributions are similar for most PDFs. The two NLO distributions stand out as two extremes in different directions where MSTW NLO has the

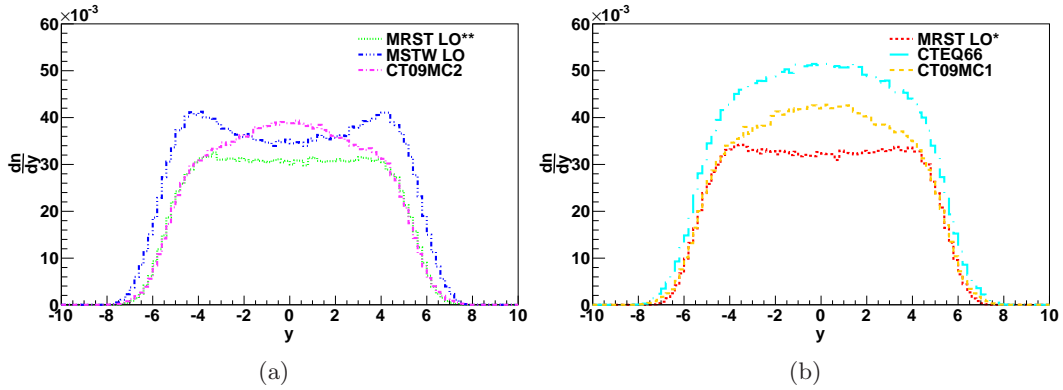


Fig. 9: Rapidity distribution for the outgoing quarks with the different PDFs. Only the $2 \rightarrow 2$ sub-process.

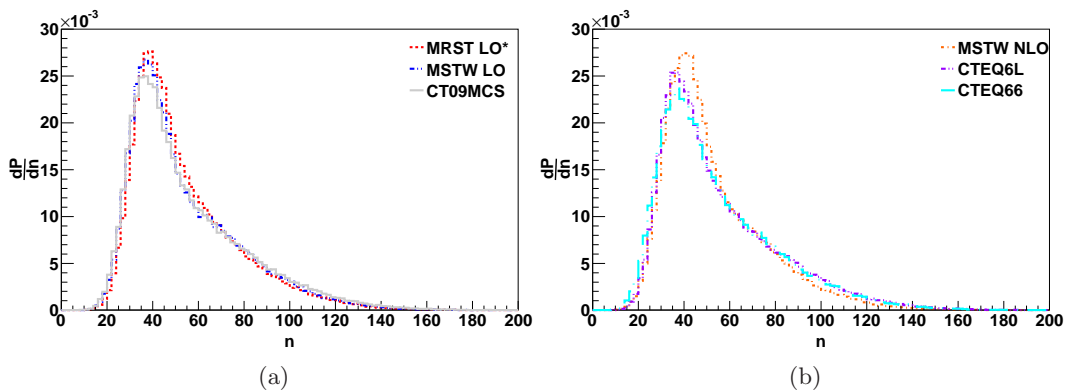


Fig. 10: Charged particle multiplicity distributions.

highest peak and the shortest tail as shown in Fig. 10. All MC-adapted PDFs except MCS have a peak slightly shifted to larger multiplicities but are different in height where the two from MRST have a larger peak value. The three normal leading-order distributions are all similar and we only show the CTEQ6L.

Fig. 11 show the p_{\perp} distribution which is almost completely independent of PDF and the overlap of the three distributions in each figure makes them impossible to distinguish.

Repeating the simulations but now with α_S set differently for the different PDFs, i.e. the value at M_Z and the order of the running is determined by the PDFs, does not significantly change anything, once the multiplicity has been returned. As an illustration of this point, the results with the two different α_S for the LO** PDF are shown in Fig. 12. CT09MCS uses a varying running of α_S which is not implemented in PYTHIA8 and the simulations with this PDF use a NLO running α_S instead. This

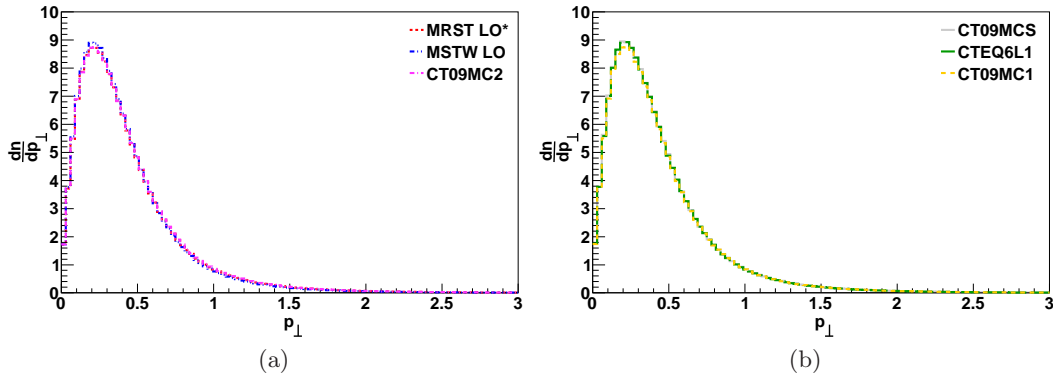


Fig. 11: p_{\perp} distributions of charged particles.

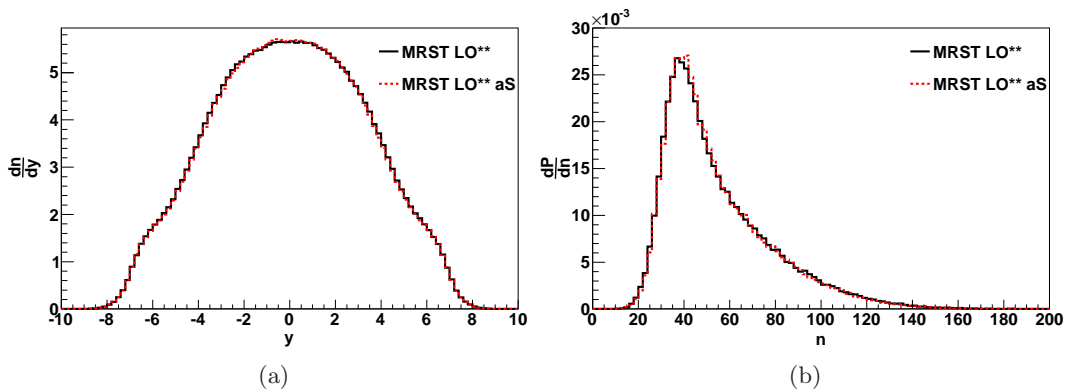


Fig. 12: MRST LO** comparison between simulations with α_S determined by PYTHIA8 and from the PDF. Rapidity distribution to the left and charge multiplicity distribution to the right. The two distributions overlap in all four figures.

should not change the results much since the varying α_S is fine tuning [35].

Increasing the energy to the level of a fully operational LHC enhances the differences seen at Tevatron energy, especially for MSTW LO and the two NLO PDFs. The multiplicity of these three evolve with energy in a different way than for the other PDFs. The rapidity distribution, shown in Fig. 13, naturally extends to larger rapidities and the total charged particle multiplicity increases since the energy available is larger. MSTW LO here gives a much broader distribution and also has a much higher total charged particle multiplicity. This is because as the energy increases even lower values of x come into play, so that the effect of the gluon distribution in this region has larger impact on the results. The two NLO PDFs have a flatter peak than the MC-adapted PDFs and are similar in shape to MSTW LO but have much smaller multiplicity. The rest of the PDFs evolve in a fashion similar to the

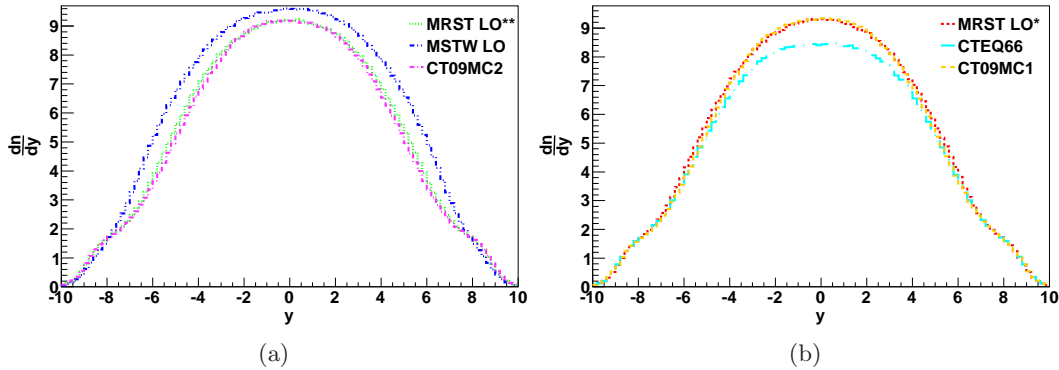


Fig. 13: Rapidity distributions at LHC ($E_{CM} = 14$ TeV).

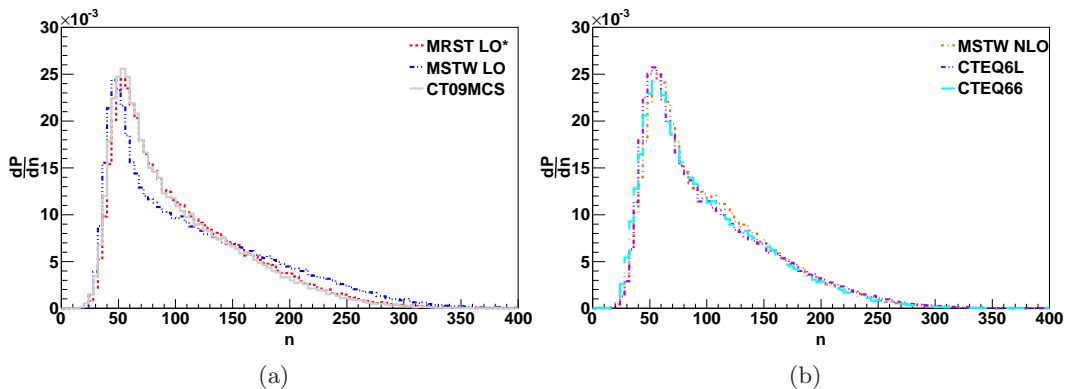


Fig. 14: Charged particle multiplicity distributions at LHC.

MC-adapted PDFs shown in the figure but with some more variation. MC1 and LO* are a little bit larger at central rapidities than MC2 and LO**.

The multiplicity distributions in Fig. 14 also show increased differences except for the two NLO PDFs which converge at this energy. Not only is there a larger mean multiplicity and peak at a higher value, but the same distributions that stand out from the rest with the rapidity also do so with their charge particle multiplicity distribution.

This is the case also for the p_{\perp} distributions but these are still very similar, excluding the MSTW LO with its large multiplicity, Fig. 15.

7.3.1 Comparison to CDF Run 2 data

The analyses in Rivet ensure that the comparisons with data have the same cuts and corrections as the original experiment. Therefore only the central pseudorapidity region is used and also cuts in transverse momentum [30]. p_{\perp} spectra of charged

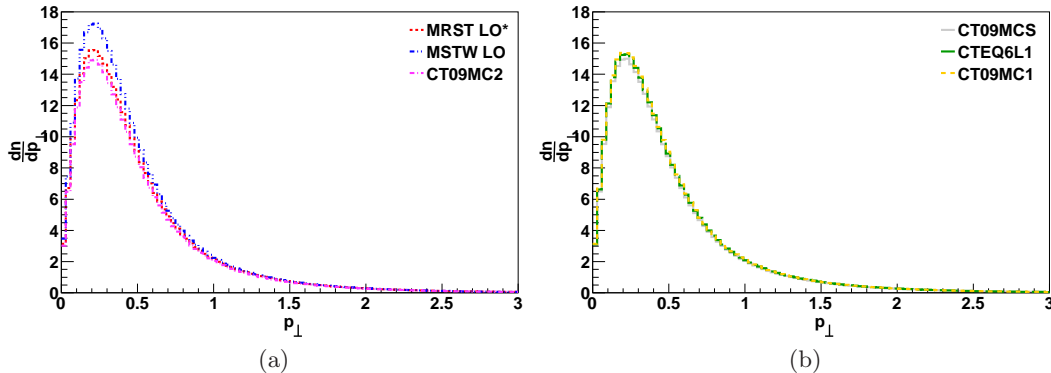


Fig. 15: p_{\perp} distributions for the different PDFs at LHC.

particles in Fig. 16 show the same relative shape for all PDFs, which gives too large values at the low p_{\perp} end, then decreases compared to data and gives too small differential cross sections at the high end. The slope shows some differences depending on the choice of PDF. MC-adapted PDFs and the CTEQ6L give results that are the closest to data, while MSTW LO and NLO are further away than the rest.

The $\sum E_{\perp}$ spectrum of particles, neutral particles included, shows larger dependence on the PDFs but it is the same distributions that result in the values closest to data. Since we have not done a complete tune, this is to indicate the importance of the PDFs and results far away from data are not necessarily the fault of the PDFs. However the $\sum E_{\perp}$ distribution is less dependent on details of the MC and therefore easier for PDF developers to consider in tunes. The MC-adapted PDFs from CTEQ as well as the CTEQ6L reproduce data well, while MSTW LO goes down to less than half the cross section of data at the larger energy end. MSTW NLO peaks at higher energies than the rest. All PDFs give a too large value at the peak, but then decrease too fast and differ the most from data at the high energy end.

Comparing the evolution of the average transverse momentum with charge multiplicity from our simulations to data (which used to be one of the distribution the MC generators struggled the most with), show that all PDFs reproduce the data fairly well and also behave in a similar fashion to one another. They all give too low $\langle p_{\perp} \rangle$ at low multiplicity and then increase relative to data so that they get closer as the multiplicity increases, Fig. 18. The only PDF that is slightly different than the rest is MSTW LO.

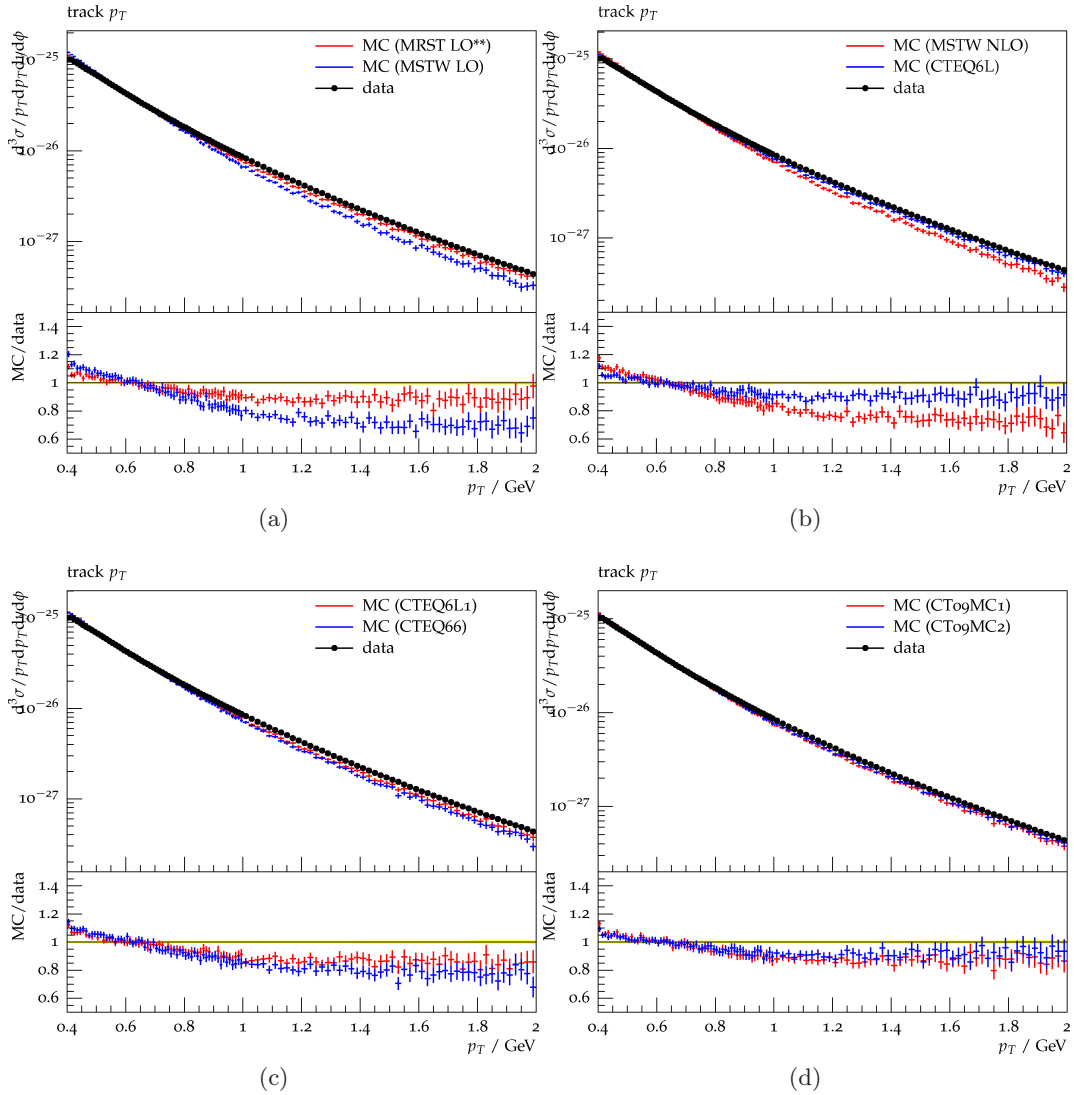


Fig. 16: p_{\perp} spectra of charged particles from the CDF Run 2 experiment compared to simulations with different PDFs.

8 Inclusive Jet Cross Section

8.1 Introduction

Quarks and gluons produced in collisions fragment because of the color confinement and produce jets of color neutral hadrons. The definition of what is a jet is far from trivial and identifying jets from data is even more difficult. This task is performed by different jet algorithms relying on closeness in either direction or momentum space.

We compare the inclusive jet cross sections from our MC simulations with data,

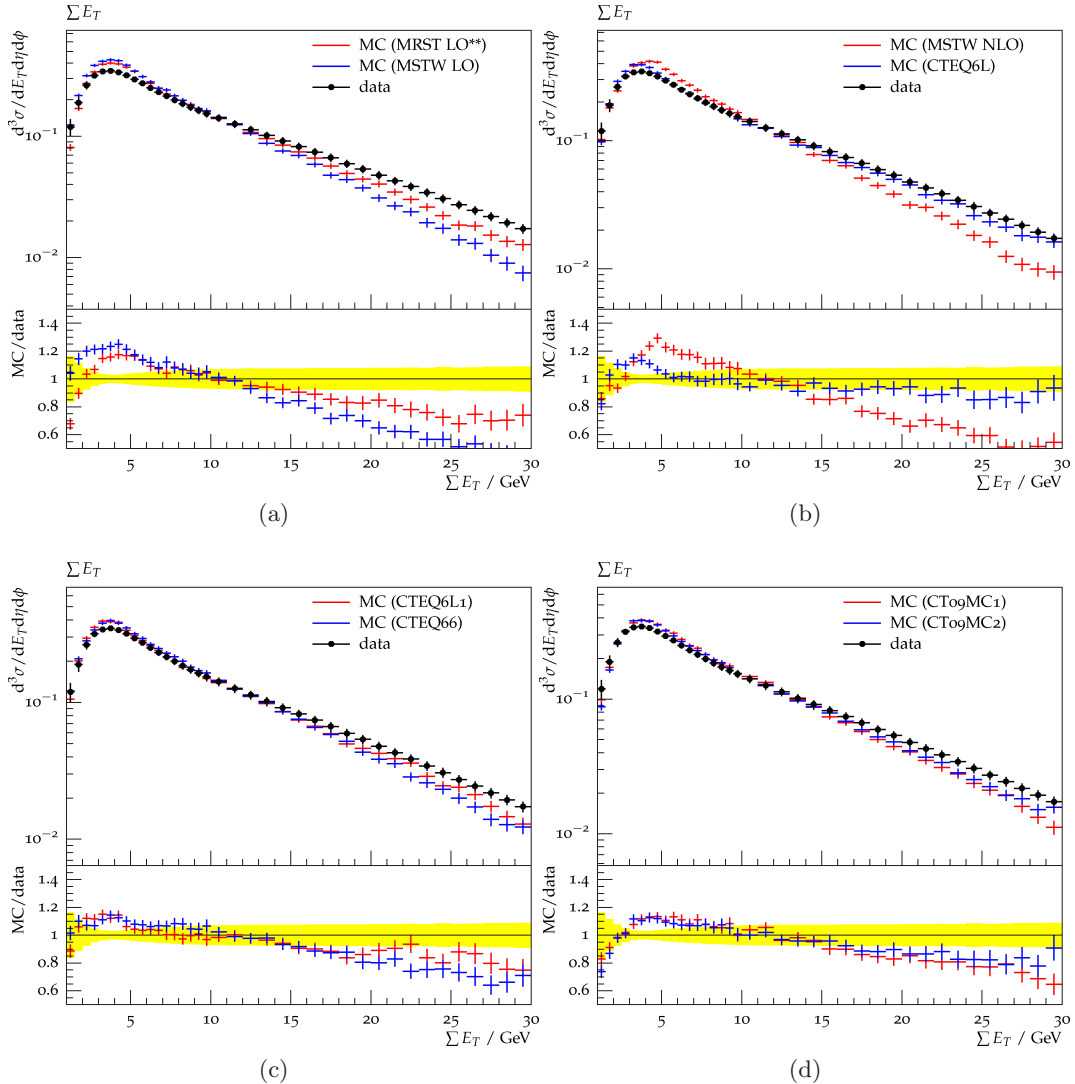


Fig. 17: ΣE_{\perp} spectra from the CDF Run 2 experiment compared to simulations with different PDFs.

collected by the CDF experiment at Tevatron Run 2 [31], over five pseudorapidity intervals ranging up to $\eta \leq 2.1$. In the experimental analysis the jets are identified with the midpoint cone algorithm and also compared to results with the k_T algorithm [32]. We are interested mainly in the low p_{\perp} region, in order to examine whether simulations can be improved by introducing a correction (K -) factor, as done, for example, in Z production. A K -factor is a factor that multiplies the cross section in order to indirectly include known corrections from next-to-leading-order calculations, and by that increase the total production rate. We also examine the rapidity, multiplicity and transverse momentum distributions for the individual hadrons. The simulations were done with a p_{\perp} cut at 40 GeV.

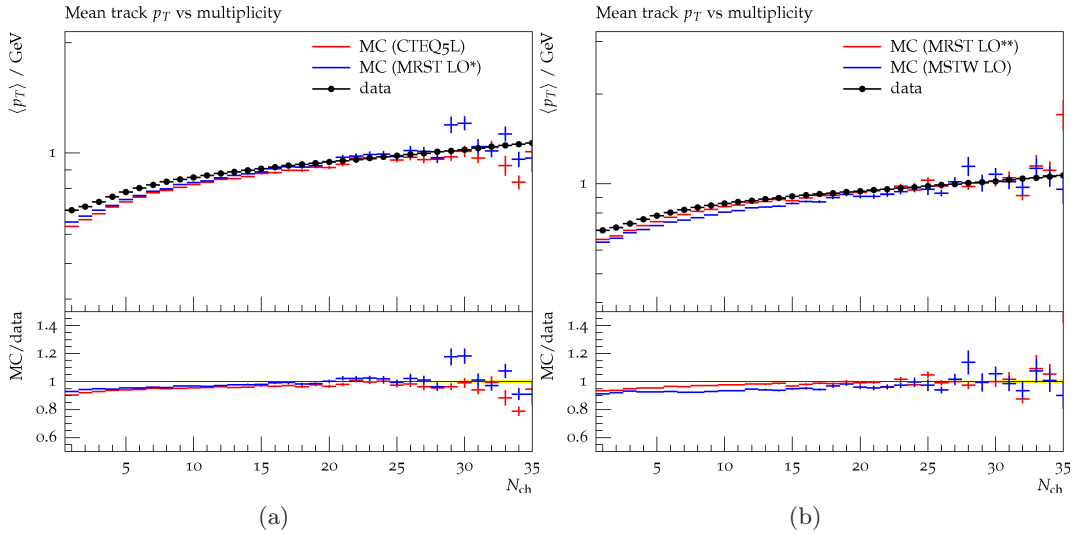


Fig. 18: Evolution of the average transverse momentum, $\langle p_T \rangle$, with charge multiplicity, N_{ch} , from the CDF Run 2 experiment compared to simulations with different PDFs.

8.2 Results

The inclusive jet cross section in Fig. 19 drops rapidly with increasing p_{\perp} and spans over several orders of magnitude. The CTEQ5L distribution, shown in Fig. 19, yields results which are lower than data, with a ratio between 0.8 and 0.9. The ratio remains fairly constant with p_{\perp} but it is closer to unity at medium pseudorapidities. Since the differences between experiments and simulations are hard to see in the main window of Fig.19 we only show the $MC/data$ ratio in the following figures. The results with MRST LO**, MSTW LO, CTEQ6L1, CTEQ66, CT09MC1 and CT09MC2 are shown in Fig. 20-22. MRST LO** starts with a much too large cross section and the ratio decreases when p_{\perp} rises. This behavior is the strongest at low pseudorapidity and as we move to larger η the ratio gets smaller and flatter. All MC-adapted PDFs, except MCS, show this type of behavior. MC2 and MC1 give results with very similar shapes but the MC2 cross section is larger. MRST LO* is related to LO** much in the same fashion as MC1 to MC2. MSTW LO and CTEQ6L give cross sections which have similar behavior as with CTEQ5L, i.e. the ratio is less dependent on p_{\perp} than with the MC-adapted PDFs. MSTW LO results are less depending on the pseudorapidity than CTEQ5L, Fig. 20. CTEQ6L1 gives a ratio which starts to decrease with p_{\perp} at larger rapidities. CT09MCS gives a too low cross section, is once again different from the other MC-adapted PDFs and gives results which behave in a way more similar to those of the normal leading-order distributions. Actually, the results with the two NLO PDFs are the closest to data at central pseudorapidities but the ratios decrease towards 0.5 at larger η .

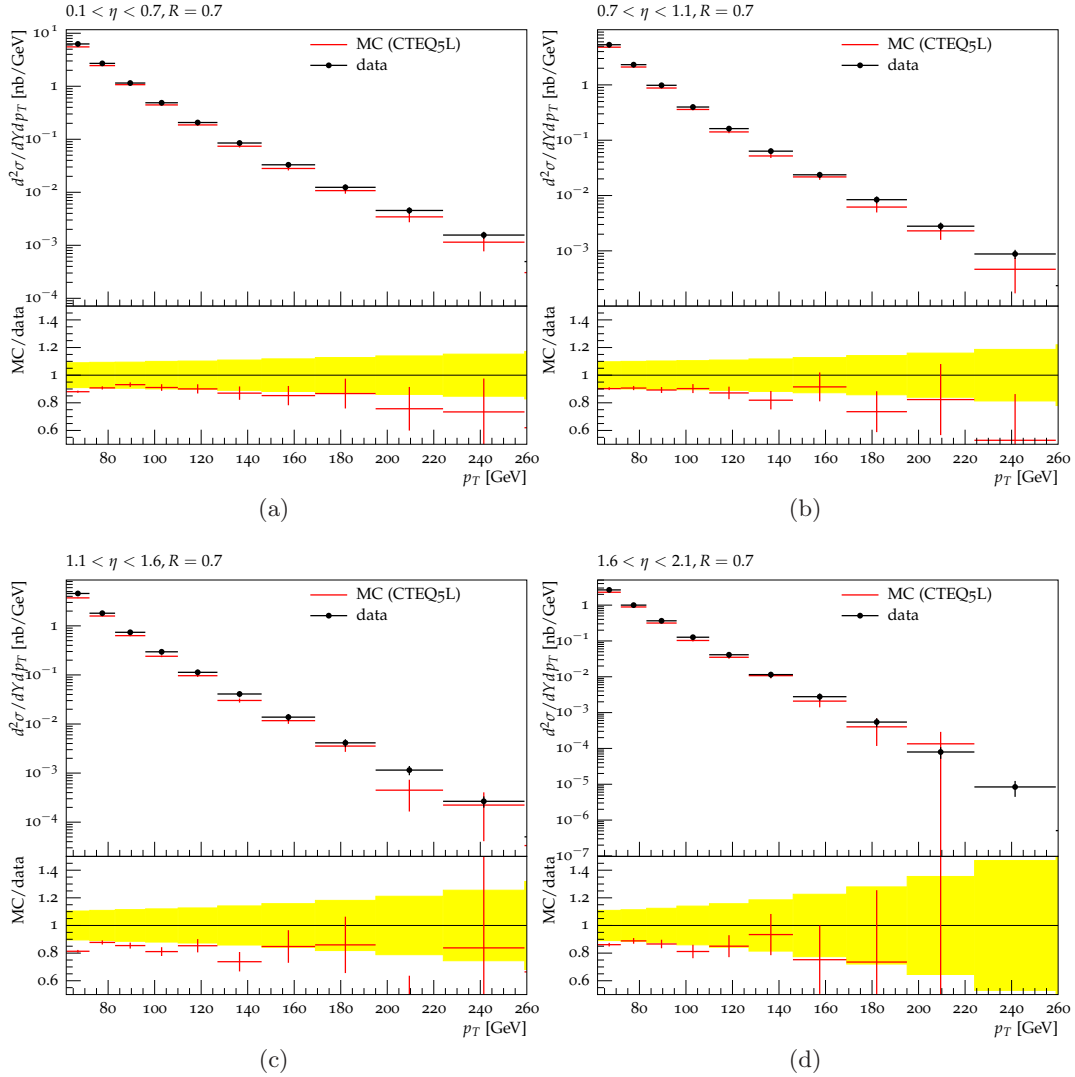


Fig. 19: Inclusive jet cross section from CDF data compared to MC simulation with the CTEQ5L PDF.

The main feature is the surprising decrease in the cross section ratio from low to high p_\perp with the MC-adapted PDFs, which we do not see with neither LO nor NLO PDFs. In order to examine the origin of this difference we look at the cross section at the parton level, after the hard collision only. Since we cannot compare to data we choose to compare to CTEQ5L, which gives a more constant p_\perp evolution of the cross section. The ratios, $R_{jet} = \sigma_{jet,PDF} / \sigma_{jet,CTEQ5L}$, in Fig. 23 show that the relative decrease with LO* and LO** is clearly visible also at parton level. This is also the case for the three MC1/2/S PDFs in Fig 23, but to less extent, while the MSTW LO results have an almost completely flat ratio. To investigate this further

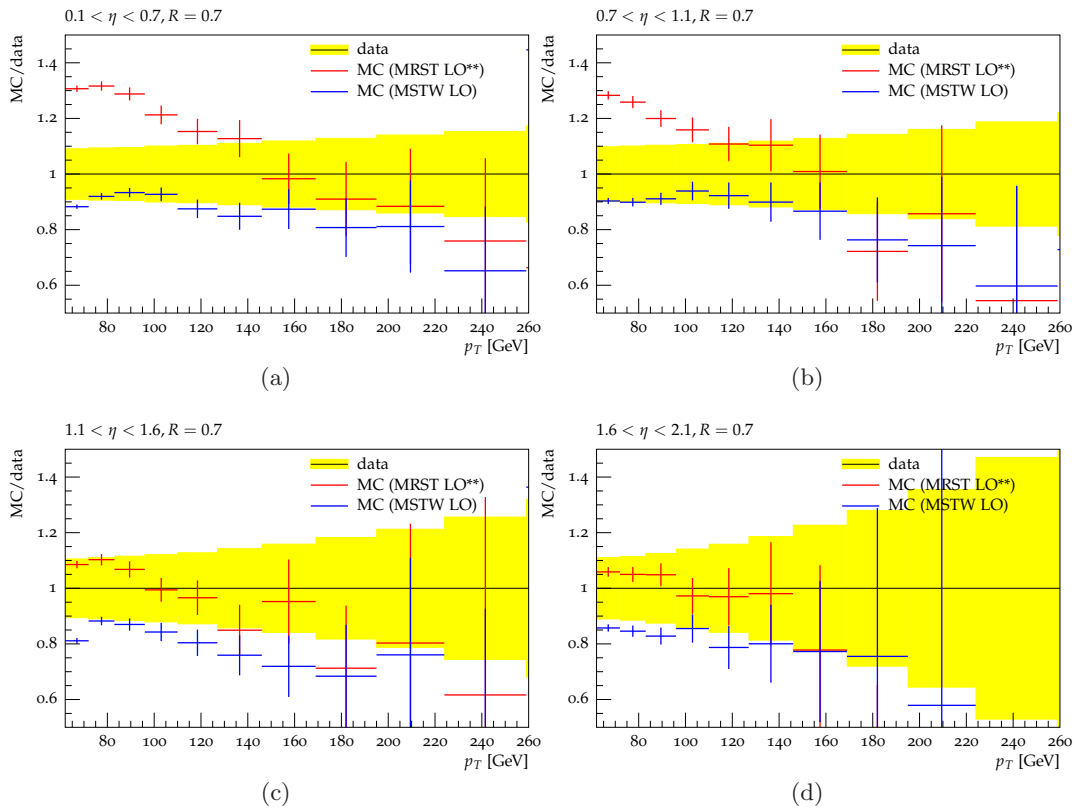


Fig. 20: Ratio of the inclusive jet cross section, MC/Data.

we integrate an approximation of the cross section

$$\frac{d\sigma}{dp_{\perp}} \sim \frac{d\hat{\sigma}}{dp_{\perp}} \sum_{ij} \int dx_1 dx_2 f_i(x_1, Q^2) f_j(x_2, Q^2) \quad (18)$$

for only the $gg \rightarrow gg$ interactions and a clear pattern very similar to the one at parton level become visible, see Fig. 24a. Fig. 24b shows that this is no longer the case if we include the other possible interactions, i.e. $qg \rightarrow qg$ and $qq \rightarrow qq$ but at the low p_{\perp} end the gluon interactions dominate.

Turning our attention to the rapidity distribution the results show less variety, see Fig.25. However, excluding MCS, all the MC-adapted PDFs give a narrower distribution. One should not be fooled by the steep slope which hides the differences. MSTW LO and NLO are smaller at central rapidities and actually have a lower multiplicity while the rest of the CTEQ distributions follow CTEQ5L. Even though the PDFs have equal charged particle multiplicity for minbias events this no longer holds true for the hard QCD events. All MC-adapted PDFs except MCS have multiplicity distributions shifted towards lower multiplicity, which is also the case for MSTW NLO and to some extent for MSTW LO, see Fig 26.

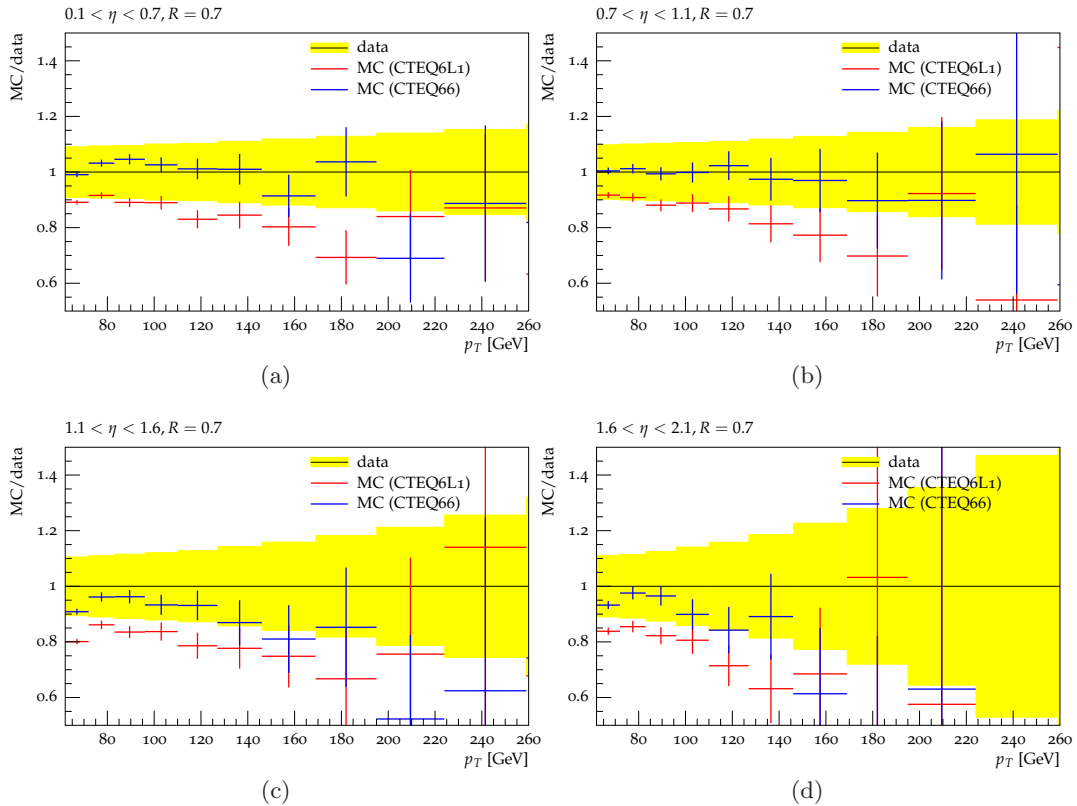


Fig. 21: Ratio of the inclusive jet cross section, MC/Data.

9 Summary and Conclusions

Including the very latest parton distribution functions into PYTHIA8 both caused some troubles and gave some surprises, especially while venturing outside the grid of the PDFs. At small x , where the gluon distribution dominates, there are large differences between the PDFs, especially at low Q^2 . The MRST/MSTW distributions are much larger than the ones from CTEQ, and MSTW LO goes sky high compared to the rest of the PDFs. At larger Q^2 the differences are smaller between the two collaborations, except for the distributions which freeze their values at the end of the grid, and for MSTW LO which is still much larger than the rest. The quarks, and in particular the up distributions, at large x show smaller differences, but MSTW LO is once again larger at small x . Some of the new MC-adapted PDFs carry a fraction of the protons momentum larger than unity, in an attempt to compensate for known shortcomings of leading-order calculations. Therefore these give a larger activity in the collisions and in order to be able to compare results from the different PDFs in simulations, we first tuned them to obtain equal charged particle multiplicity.

The different behavior for MSTW LO was also reflected in rapidity distributions both at the level of the $2 \rightarrow 2$ sub-process and after hadronization. In general the

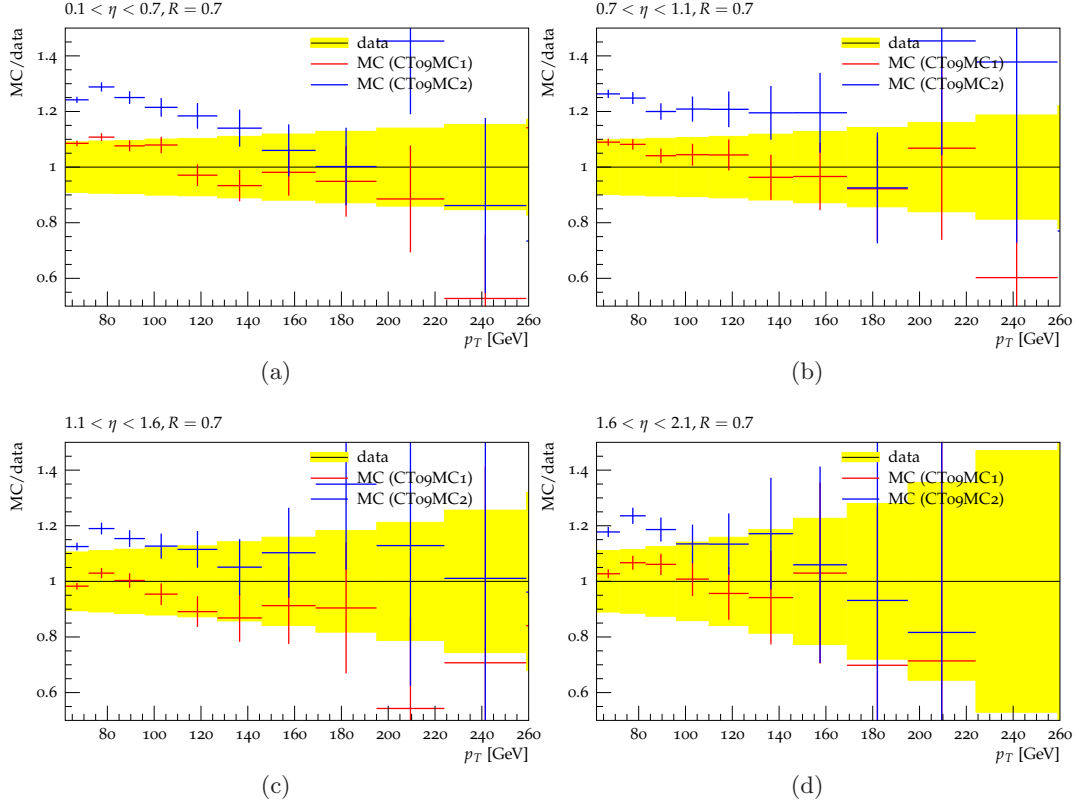
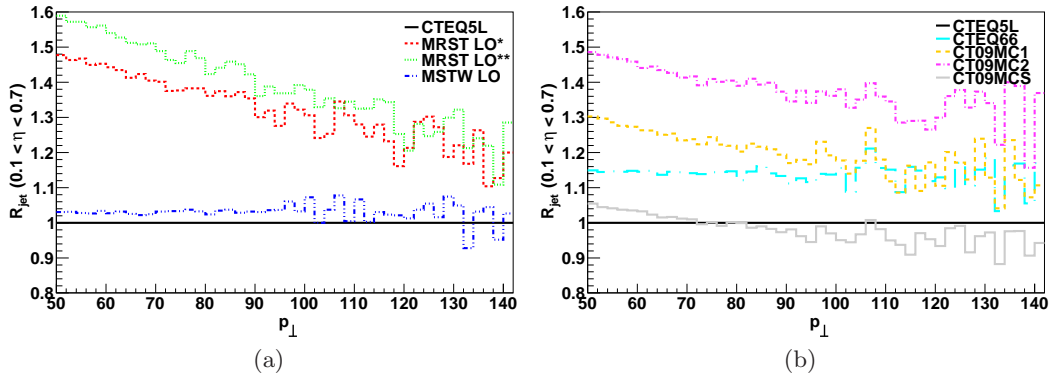


Fig. 22: Ratio of the inclusive jet cross section, MC/Data.

Fig. 23: Ratio of cross section for the $2 \rightarrow 2$ sub-process with the different PDFs over cross section with CTEQ5L.

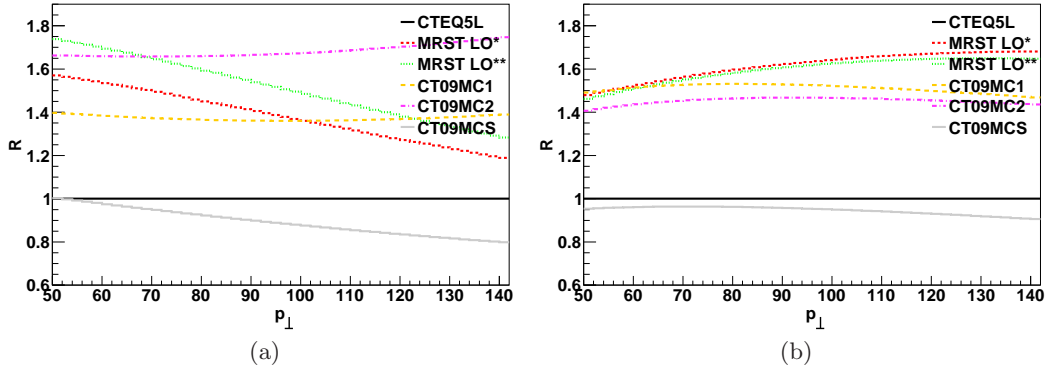


Fig. 24: Ratio of the approximated cross section with different PDFs to CTEQ5L. Left figure show only the gg interactions while the right figure also include gg and qq interactions.

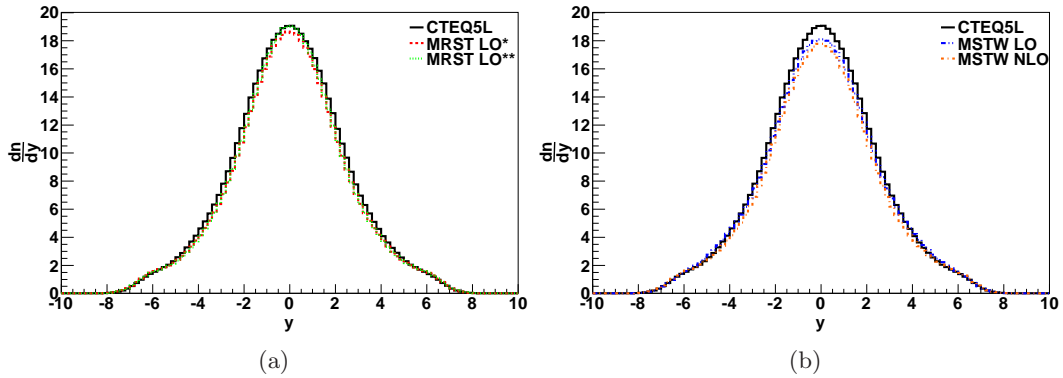


Fig. 25: Hard QCD rapidity distributions.

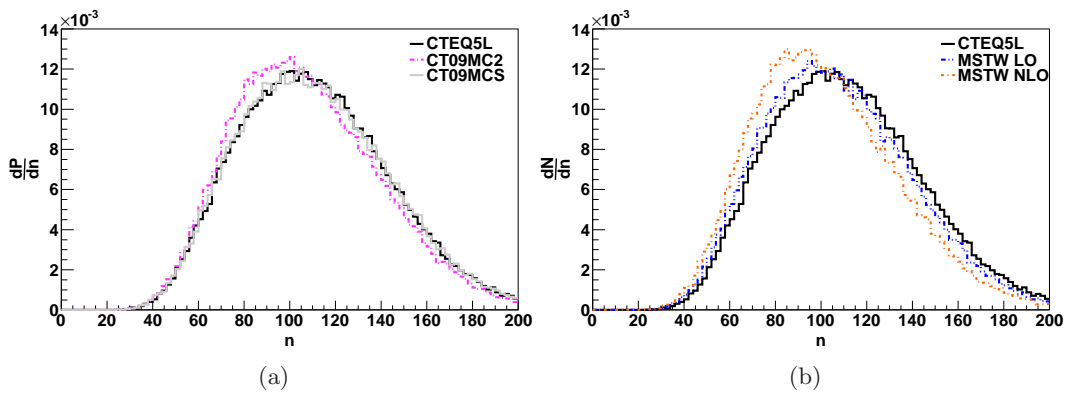


Fig. 26: Hard QCD multiplicity distributions.

differences in the PDFs are blurred down to parton level and then blurred even more at hadron level, but some large differences still remain. By comparison to minimum bias data from CDF we saw that the MC adapted PDFs gave similar results and were in general closer to data than the LO and NLO PDFs, with the exception of CTEQ6L. Differences between the results with different PDFs were enhanced when the energy was increased up to the LHC level. We also discovered that the multiplicity evolved differently with MSTW LO and with the two next to leading-order PDFs than with the rest.

In the simulations of hard QCD events we saw that the rapidity distributions with the MC-adapted PDFs were narrower, and that their multiplicity distributions were shifted to lower multiplicity. The evolution of the differential jet cross section with p_{\perp} was found to be strongly dependent on the choice of PDF, both when it came to its size and shape. In the simulations of hard events we saw that the rapidity distribution was narrower for the MC-adapted PDFs and that their multiplicity distributions shifted to lower multiplicity. The evolution of the cross section with p_{\perp} was strongly dependent on the PDF. Comparing the p_{\perp} spectrum ratio (simulation over data) the MC-adapted PDFs showed a rather surprising change in ratio with p_{\perp} which we examined further. The same behavior could be seen at the level of the $2 \rightarrow 2$ sub-process as well and this was traced to the $gg \rightarrow gg$ interactions, that dominate in this region. The changes in behavior for the inclusive jet cross section with different PDFs can also be caused by the change of dominating process in the p_{\perp} , from $gg \rightarrow gg$ to $qg \rightarrow qg$. Simulations of prompt photon production also showed such decrease in the cross section for gg but not for qg nor qq interactions.

There is a need for better understanding of parton distribution functions at small x where the PDFs are now very different from each other. In minbias events x values of the order of $10^{-6} - 10^{-4}$ are the most common. MC simulations need the PDFs to range down to $x = 10^{-8}$ which so far only the three brand new CT09 PDFs do, and we would therefore like to encourage MSTW to extend their grid for the MC-adapted PDFs in their next release. At several occasions we were reminded that it can be risky to use NLO PDFs in LO MC generators. Our implementation of LO* and LO** with the new grid causes these two distributions to have a smaller gluon distribution at small x , but would otherwise give results more similar MSTW LO. In addition we found that there is a need for improved numerical stability at large x in order to keep the leading-order PDFs from going negative. This could possibly be solved by using less intricate interpolation routines in this area. Possibly one could choose an x_{max} , different for sea-quarks, gluons and valence quarks, above which one uses the form $N(1-x)^p$ where N and p are functions of the virtuality, which would ensure positivity. The large differences in the PDFs get blurred when looking at simulation results, but nonetheless do sometimes cause large variations.

Changing from the default α_S behavior in PYTHIA8 to α_S value and running determined by the PDFs did not change the results, once the multiplicity had been returned.

Interesting to note is that the CT09MCS seems to have some of the features of the other MC-adapted PDFs but in some contexts gives results more similar to

ordinary leading-order PDFs. The difference in quark rapidity between MC1/2/S and the rest could be due to their fitting to the NLO pseudo data. The only two other distributions with similar shape are the two NLO PDFs.

We could see that a K -factor for the leading-order PDFs could improve the fit to the inclusive jet data, but for the MC-adapted PDFs the change of the ratio makes it more complicated. Finally, the differences in the PDFs have a larger impact when the CM-energy of the collisions increases, and this can cause large uncertainties in simulations at LHC energies.

At this point no final answer as to which PDF gives the best results. In order to answer this question one has to look at a much broader spectrum of observables and also make complete tunes for the different PDFs.

In the last years there has been a renewed interest in LO tunes with focus on the applicability in MC generators. The MC-adapted PDFs resulted in some very interesting differences compared to leading-order PDF but there is still room for further improvements. With these new PDFs we have gained a broader spectrum of tools in PYTHIA8 and in examining the origin of differences and similarities between simulations and experiments.

10 Acknowledgments

First and foremost I want to thank my supervisor Torbjörn Sjöstrand for his help and ability to explain difficult things in an understandable way. I also owe many thanks to Leif Lönnblad, Hendrik Hoeth and all the other people at the department of Theoretical Physics, as well as to Marianne Döös, Sanne Kasemets and Julia Kryszewska. I would also like to mention Johan Bijnens, Joakim Cederkäll, Bo Söderberg and Hans-Uno Bengtsson who all played an important role in my previous education.

References

- [1] T. Sjöstrand, S. Mrenna and P. Skands, *Comput. Phys. Commun* **178** (2008) 852-867 [arXiv:hep-ph/0170.3820].
- [2] Tevatron, <http://www-bdnew.fnal.gov/tevatron/>.
- [3] LHC, <http://lhc.web.cern.ch/lhc/>.
- [4] See e.g. M. E. Peskin and D. V. Schroeder, *An Introduction to Quantum Field Theory* (Westview Press, USA, 1995).
- [5] J. M. Campbell, J. W. Huston and W. J. Stirling, *Rept. Prog. Phys.* 70, 89 (2007) [arXiv:hep-ph/0611148].
- [6] See e.g. R. K. Ellis, W. J. Stirling and B. R. Webber, *QCD and Collider Physics* (Cambridge University Press, United Kingdom, 1996).

-
- [7] M. A. Dobbs et.al., (2004) [arXiv:0403045v2] .
- [8] N. Lavesson, *Merging Parton Showers and Matrix Elements* (PhD thesis, Lund University, 2009).
- [9] T. Sjöstrand, *Phys.Lett.* **B157** (1985) 321.
- [10] T. Sjöstrand, *Monte Carlo Generators* (2006) [arXiv:hep-ph/0611247v1].
- [11] C. Friberg and T. Sjöstrand, (2004) [arXiv:hep-ph/9906316].
- [12] T. Sjöstrand, S. Mrenna, and P. Skands, *JHEP* **05** (2006) 026 [arXiv:hep-ph/0603175].
- [13] G. Corcella et.al., *JHEP* **0101** (2001) 010 [arXiv:hep-ph/0011363].
- [14] B. Andersson, G. Gustafson, G. Ingelman and T. Sjöstrand, *Phys.Rept.* **97** (1983) 31.
- [15] B. R. Webber, *Nucl. Phys.* **B238** (1984) 492.
- [16] H. Chen, F.-G. Cao and A. I. Signal, (2009) [arXiv:hep-ph/0912.0351v1].
- [17] A. D. Martin, *Acta Phys. Polon.* **B39** 2025-2062, (2008) [arXiv:hep-ph/0802.0161v1].
- [18] A. D. Martin, W. J. Stirling, R. S. Thorne and G. Watt, *Eur. Phys. J.* **C63** (2009) 189 [arXiv:hep-ph/0901.0002].
- [19] J. Pumplin, D. R. Stump, J. Huston, H. L. Lai, P. Nadolsky and W. K. Tung, *JHEP* **0207** (2002) 012 [arXiv:hep-ph/0201195].
- [20] J. Kretzschmar, [H1/ZEUS Collaboration], [arXiv:hep-ex/0906.1108]. A. Cooper Sarkar, talk at *SM and BSM physics at the LHC*, Aug.6 2009, CERN.
- [21] R. D. Ball et al. [NNPDF Collaboration], *Nucl. Phys.* **B809** (2009) 1 [arXiv:hep-ph/0808.1231].
- [22] J. Huston, *ATL-PHYS-99-008* (1999).
- [23] A. Sherstnev and R. S. Thorne, (2008) [arXiv:0807.2132v1].
- [24] A. Sherstnev and R. S. Thorne, *Eur. Phys. J.* **C55**, 553 (2008) [arXiv:hep-ph/0711.2473].
- [25] H. L. Lai, J. Huston, S. Mrenna, P. Nadolsky, D. Stump, W. K. Tung and C. P. Yuan, (2009) [arXiv:hep-ph/0910.4183].
- [26] M. Glueck, E. Reya and A. Vogt, *Z.Phys.* **C67** (1995) 433.

- [27] H. L. Lai et al. [CTEQ Collaboration], *Eur. Phys. J.* **C12** (2000) 375
- [28] LHAPDF, <http://hepforge.cedar.ac.uk/lhapdf/>.
- [29] Rivet, <http://projects.hepforge.org/rivet/>.
- [30] T. Aaltonen et al. [CDF Collaboration], *Phys. Rev.* **D79** (2009) 112005.[arXiv:0904.1098v2].
- [31] T. Aaltonen et al. [CDF Collaboration], *Phys. Rev.* **D78** (2008) 052006 [arXiv:hep-ph/0807.2204].
- [32] G. P. Salam, (2009) [arXiv:hep-ph/0906.1833v1].
- [33] Correspondence R. Thorne
- [34] Correspondence S. Mrenna
- [35] Correspondence J. Huston